CHEMISTRY OF MATERIALS

Communication

pubs.acs.org/cm

Employing Overlayers To Improve the Performance of Cu_2BaSnS_4 Thin Film based Photoelectrochemical Water Reduction Devices

Jie Ge,*[,†] Paul J. Roland,[†] Prakash Koirala,[†] Weiwei Meng,[†] James L. Young,[‡] Reese Petersen,[‡] Todd G. Deutsch,[‡] Glenn Teeter,[‡] Randy J. Ellingson,[†] Robert W. Collins,[†] and Yanfa Yan*[,†]

[†]Department of Physics and Astronomy & Wright Center for Photovoltaics Innovation and Commercialization, The University of Toledo, Toledo, Ohio 43606, United States

[‡]National Renewable Energy Laboratory, Golden, Colorado 80401, United States

Supporting Information

Solar energy sources, such as hydrogen fuel produced by photoelectrochemical (PEC) water splitting, offer the promise of essentially limitless clean energy for powering our society. Achieving high efficiency for solar-to-hydrogen conversion is essential for reducing the cost of these technologies. The tandem device concept of stacking a wide-bandgap and a narrow-bandgap semiconductor is a proven method for producing high conversion efficiency in PEC devices.[1]

However, to date, most devices that successfully employ this technique can only be produced using III−V epitaxial thin films. The complexity of epitaxial growth procedures and their use of expensive single-crystal substrates have prevented the III−V tandem devices from achieving low cost. In contrast to epitaxial III−V devices, polycrystalline thin−film devices offer much lower production cost and complexity but typically yield devices with only moderate efficiencies. Combining the tandem cell concept with low-cost polycrystalline thin films would be an ideal choice for next-generation PEC devices. Unfortunately, high-efficiency tandem polycrystalline thin-film PEC devices remain challenging to realize, largely because of the lack of promising top cells using wide-bandgap semiconductor absorbers.[2−4] Cu_2O, with a bandgap E_g ∼2 eV, has already attracted attention for PEC water splitting and photovoltaic (PV) applications due to its earth-abundance and non-toxicity.[5−7] Its wide bandgap enables Cu_2O with the ability to act as a top cell in the tandem PEC solar cell and in the PEC/PV integrated solar cell to serve to split water[8,9] but has not yet been fully optimized for these applications, due to its low photocurrents.

Recently, density-functional theory (DFT) calculation results suggest that trigonal copper−barium−thiostannate Cu_2BaSnS_4 (CBTS), an earth-abundant wide-bandgap semiconductor, together with its selenide counterpart $Cu_2BaSnSe_4$, presents optoelectronic and defect properties suitable for top cell candidates for tandem PEC and PV applications.[10,11] Like $CuInSe_2$ and CZTS, the valence band of CBTS contains Cu d^{10} states, leading to high joint density of states and therefore high optical absorption coefficients in the visible light range. Due to the large mismatch on size and electronic properties between Cu and Ba and Sn cations, the dominant defect is the Cu vacancy in CBTS, which creates a shallow acceptor state.[10] This is similar to the defect properties in $CuInSe_2$ but not those found in CZTS due to Cu and Zn ions which are the nearest neighbors on the periodic table and have similar size.[12] Thus, CBTS is expected to exhibit low density of nonradiative recombination centers, and its solar cell is expected to show fewer losses in photovoltage and photocurrent.

The earliest report on CBTS was published by Teske et al. in 1976, where CBTS was identified to adopt a trigonal structure with a space group of $P3_1$.[13] In 2014, Chorkendorff et al. predicted that the bandgap of CBTS (1.5 eV ≤ E_g ≤ 2.1 eV) could be suitable as a top-cell absorber in tandem PEC cell applications.[14] Until recently, some basic material properties of CBTS (e.g., bandgap E_g ∼ 2 eV) and its applications in PEC and PV solar energy conversion have just been investigated in experiments.[15−18] Our Mott−Schottky analyses have estimated that the conduction band and valence band of CBTS straddle the water reduction and oxidation potentials, so that photocarriers can travel to the CBTS−electrolyte junction and react with water.[16−18] Our previous PEC tests have shown that a pristine CBTS thin film could generate a photocurrent of ∼5 mA cm^{-2} with a late onset potential toward water reduction,[17] which is not satisfactory to make CBTS to serve as an efficient top cell in a tandem PEC cell. Incorporating selenium into CBTS could reduce the bandgap and increase the photocurrent;[17,19] however, the use of selenium will cause a cost hike on device manufacture due to its limited storage in earth's crust and small volume of production.[20] According to the Shockley−Queisser theory, CBTS can generate a photocurrent of ∼14.5 mA cm^{-2} under one sun illumination,[21] which is much larger than our best experimental result based on pristine CBTS thin film based photoelectrode. Furthermore, bare CBTS may not be stable in electrolytes, which can in turn limit the photocurrent. Therefore, there is much room for photocurrent boosting in experiments.

Here, we report that employing CdS/ZnO/TiO_2 overlayers on the CBTS surface can effectively enhance the photocurrents and improve the device stability. CdS/ZnO or CdS can form p−n junctions with p-type chalcogenide absorbers, which can build a more robust built-in field in the junction region than the absorber−electrolyte interface. This robust built-in field can induce a greater band bending and extend the depletion width deep into the absorber, which is beneficial to enhance the charge separation.[22−24] Compared to other *n*-type semi-

Received: August 12, 2016
Revised: January 18, 2017
Published: January 19, 2017

DOI: 10.1021/acs.chemmater.6b03347
Chem. Mater. XXXX, XXX, XXX−XXX

conductors such as ZnO, the CdS buffer additionally shows a smaller lattice mismatch with the Cu-based chalcogenide absorbers;[18] therefore, CdS will lead to a lower defect density at the buffer/absorber interface,[25] alleviating the photocarrier recombination at the buffer/absorber interface. However, CdS and ZnO are susceptible to photocorrosion during water splitting. The TiO_2 top layer can inhibit the device from corrosion by contact with the electrolyte solution.[26−28] The CBM positions of ZnO and TiO_2 are appropriate for effectively transferring electrons to electrolyte solution.[5,24] As a result, the best saturated cathodic photocurrent is enhanced to 7.8 mA cm^{-2} at the potential of −0.10 V versus reversible hydrogen electrode (RHE) in a neutral electrolyte solution, as compared to the best bare CBTS thin film attaining a photocurrent of 4.8 mA cm^{-2} at the potential of −0.2 V versus RHE. These results strongly suggest that earth-abundant CBTS is a promising candidate as a top-cell absorber for efficient and low-cost tandem polycrystalline thin-film PEC devices, and overlayers can be employed to enhance device photocurrent, onset potential, and stability.

Our CBTS thin films were prepared by co-sputtering of Cu, SnS, and BaS targets on the fluorine doped tin oxide (FTO) coated soda lime glass substrates (for device fabrication) or fused silica glass substrates (for characterization) and followed by sulfurization annealing at 540 °C in sulfur vapor. Panels (a) and (b) of Figure 1 show the top-view scanning electron microscopic (SEM) images of two sulfurized CBTS films deposited on a fused silica substrate and an FTO coated glass substrate, respectively. It is seen that the sulfurized CBTS films deposited by co-sputtering method are pinhole-free and compact without any secondary phases, with grain sizes varying from 0.2 to 1.2 μm. Figure 1b shows the Bragg−Bretano θ−2θ X-ray diffraction (XRD) patterns of a CBTS film deposited on fused silica and a CBTS film deposited on an FTO substrate after sulfurization. The XRD patterns show high crystallinity of the films with all peaks assignable to the trigonal CBTS (PDF 97-005-2685) or FTO (marked by "*") phases. The positions of these major reflections along with the calculated lattice constants of a = 6.367 Å and c = 15.833 Å agree quite well with those from trigonal CBTS (PDF 97-005-2685). Figure 1d shows the optical transmission spectra of these two CBTS films measured by ultraviolet−visible (UV−vis) spectroscopy. In the IR spectral region, the film deposited on the fused silica substrate demonstrates a high average optical transmittance (>70%), indicating that CBTS film is insulating, while the low IR transmittance (<20%) of the film deposited on the FTO substrate suggests that FTO remains suitably conductive after sulfurization. Sharp cut-offs at 2.0−2.1 eV in the transmission spectra indicate the bandgap of CBTS. A direct transition plot of $(\alpha E)^2$ vs E in the Figure 1d inset leads to a 2.046 eV bandgap for CBTS. The CBTS film deposited on a fused silica substrate shows very similar XRD and the same bandgap value with the one on the FTO substrate, suggesting no reaction between CBTS films and FTO substrates, which is important for PEC device fabrication.

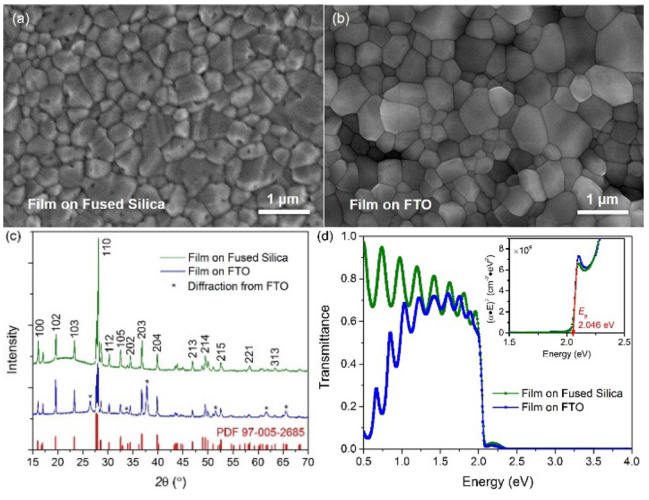

Figure 1. (a and b) top-view SEM images, (c) XRD patterns, and (d) optical transmittance spectra and bandgap plots of two 1200 nm thick CBTS films grown on a fused silica substrate and an FTO coated glass substrate. Note: the peaks marked by "*" in panel (c) at 2θ = 26.500°, 33.738°, 37.800°, 51.400°, 61.581°, and 65.540° correspond to the (110), (101), (200), (211), (310), and (301) reflections of the FTO substrate (SnO_2, PDF 97-026-2768), respectively; the remaining peaks are indexed to Cu_2BaSnS_4 (red markers, PDF 97-005-2685, space group $P3_1$); in panel (d) inset, the absorption coefficient $\alpha = \frac{1}{d}\ln\left(\frac{1}{T}\right)$, where d is the film thickness and T is the film transmittance.

Our DFT calculation using the HSE06 hybrid functional shows that CBTS should exhibit a nearly direct bandgap (Figure S1a). To reproduce the experimental bandgap of 2.053 eV (to be shown below), we find that a large portion (37%) of the exact Hartree−Fock exchange is needed. The calculated partial density of states (PDOS) (Figure S1b) shows that the valence band of CBTS is composed of anti-bonding states from Cu 3d and S 3p orbitals, while the conduction band minimum (CBM) is mainly derived from Sn 5s and S 3p orbitals.

The CBTS film grown on the fused silica substrate was additionally characterized by spectroscopic ellipsometry (SE). A layer thickness of 1200 nm was determined by SE. The SE-derived absorption coefficient α and dielectric function of CBTS are shown in Figure 2a and Figure S2, respectively. The solid line in Figure 2a and Figure S2 is a parametrized model based on a sum of critical point oscillators,[18] which reveals a bandgap critical point (CP) of 2.053 eV (E_0) corresponding to the exact fundamental bandgap of CBTS. The CBTS exhibits a strong absorption coefficient, $\alpha > 10^4$ cm^{-1}, for the range of the photon energies E > 2 eV. Using the SE-derived absorption coefficient α, a direct transition plot of $(\alpha E)^2$ vs E in Figure 2a inset leads to a 2.046 eV bandgap for CBTS, agreeing quite well with the results shown in the Figure 1d inset. The absorption coefficient (or ε_2 in Figure S2a) exhibits a strong local maximum at the CP of E_1 = 2.353 eV.

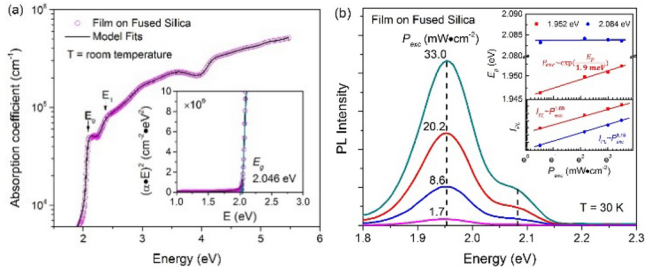

Figure 2. (a) Spectroscopic ellipsometry (SE) measured absorption coefficient and bandgap plot (inset) at room temperature and a best fit model based on a sum of critical point oscillators and (b) excitation-intensity dependent photoluminescence (PL) spectra at 30 K of an 1200 nm thick CBTS film deposited on a fused silica substrate.

DOI: 10.1021/acs.chemmater.6b03347
Chem. Mater. XXXX, XXX, XXX−XXX

Figure 2b shows the photoluminescence (PL) spectra of the 1200 nm thick CBTS film deposited on the fused silica substrate with various illumination power densities at 30 K. The PL curves show a maximum at 1.952 eV with a 110 meV line width along with a shoulder peak at 2.084 eV with a 70 meV line width. No apparent energy position (E_p) shift was observed for the 2.084 eV PL peak over the range of excitation powers (P_{exc}) used, and the exponent of $k = 1.18 \pm 0.02$ was determined from the exponential relation $I_{PL} \sim P_{exc}{}^{k}$ where I_{PL} is energy-integrated luminescence intensity. These characteristics are consistent with a near-band-edge bound exciton transition.[29−31] The fit using the exponential dependence of $P_{exc} \sim \exp\left(\frac{E_p}{\beta}\right)$ yields the energy shift constant $\beta = 1.9$ meV/decade for 1.952 eV emission, which is consistent with either a free-to-bound (FB) or a donor−acceptor pair (DAP) transition.[32,33] The maximum Coulomb-energy related shift of DAP transitions, $E_{max} \sim 153$ meV, can be estimated from the binding energy of the spatially extended defect, usually the donor level, using the hydrogenic impurity model given by $E_{max} = \frac{m_e^* e^4}{2(4\pi\varepsilon_0\varepsilon_r\hbar)^2}$,[31] where the electron effective mass $m_e^* \approx 0.33m_0$ (Table S1) and the relative dielectric constant $\varepsilon_r \approx 5.4$ for CBTS. The 1.952 eV emission peak shift of ∼6 meV is smaller than the energy shift expected for DAP recombination. Thus, we tentatively attribute the 1.952 eV emission to a FB transition corresponding to relaxation from the conduction band to an acceptor level (e−A^0) for p-type CBTS. Although the k value of 1.08 ± 0.05 extracted from a linear fit to $I_{PL} \sim P_{exc}{}^{k}$ is slightly larger than 1, this behavior has been previously reported for impurity-related PL emission.[33,34] The observation of the slight peak shift and small peak energy difference relative to the bandgap for 1.952 eV emission suggest that the dominant defects in CBTS are shallower defects and that CBTS shows less defect-related compensation than CZTS.[34,35] This is consistent with the theoretical prediction that the shallow Cu vacancy (V_{Cu}) defect is dominant in CBTS.[10]

Panels (a) and (b) of Figure 3 show the cross-sectional SEM images at different magnifications of a finished CBTS PEC device coated with CdS/ZnO/TiO_2 overlayers. The CdS layer was deposited by RF sputtering at 150 °C, while the ZnO and TiO_2 thin layers were deposited by oxygen-plasma-enhanced atomic layer deposition at 200 °C. Figure 3a shows that the layer thickness of CBTS is 1100−1200 nm, consistent with the thickness value determined by SE. Large CBTS grains extend through the entire layer thickness. No secondary phase segregates at the rear side of CBTS absorber, confirming again that there is no reaction between CBTS and FTO substrate. The magnified cross-sectional SEM image in Figure 3b shows no-grain morphology of the TiO_2 layer, indicating an amorphous nature, while the ZnO and CdS thin layers are crystalline. Notably, the p−n junction of CBTS/CdS/ZnO is contiguous and uniform, and the protection layer TiO_2 is conformal and pinhole-free, both of which are the most important parameters for a high performance CBTS PEC device.

Our PEC devices using bare CBTS electrodes generated cathodic photocurrents under illumination, indicating that sulfurized CBTS thin films act as photocathodes and the films could have a p-type conductivity. The saturated photocurrent of 4.8 mA cm^{-2} was reached at the potential of −0.2 V versus RHE for a FTO/CBTS/electrolyte PEC cell measured in a neutral solution (pH ∼ 7) using a Xe light source

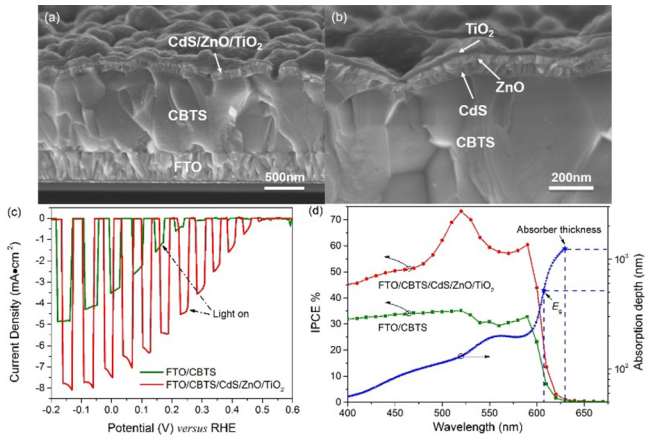

Figure 3. (a) Cross-sectional SEM image of a completed glass/FTO/CBTS/CdS/ZnO/TiO_2 PEC device prior to PEC testing; (b) magnified cross-sectional SEM image showing the structural detail at the interface of CBTS/CdS/ZnO/TiO_2; (c) linear sweep voltammetry (LSV) scanning curves of glass/FTO/CBTS/electrolyte and glass/FTO/CBTS/CdS/ZnO/TiO_2/electrolyte PEC cells under manually chopped light; (d) IPCE spectra measured at the potential of 0 V versus RHE and the absorption depth ($1/\alpha$) of CBTS. The photoelectrodes were processed with a 1 mM chloroplatinic solution prior to PEC testing. All the measurements were carried out using a three-electrode configuration in a neutral electrolyte (pH ∼ 7).

equipped with a 420 nm cutoff filter, as shown by the green curve plotted in Figure 3c. The photocurrent onset potential of +0.25 V versus RHE suggests a large over potential for the CBTS/electrolyte interface. To help extract electrons and transfer them to the electrolyte solution, we modified the CBTS surface by depositing CdS/ZnO/TiO_2 thin layers. As shown by the red curve in Figure 3c, the addition of the CdS/ZnO/TiO_2 layers significantly improves the saturated photocurrent up to 7.8 mA cm^{-2} at the potential of −0.1 V versus RHE and anodically shifts the photocurrent onset with respect to that of the FTO/CBTS/electrolyte device. Copious hydrogen bubbles were observed during PEC tests of bare CBTS and CBTS/CdS/ZnO/TiO_2 electrodes (Figure S3).

The incident photon to current efficiency (IPCE) measurement was carried out at the potential of 0 V versus RHE to show the spectral distribution of photocurrent generation (Figure 3d). IPCE results indicate that the photocurrent is from the CBTS absorber. The absorption depth ($1/\alpha$), which was calculated from the SE-derived absorption coefficient α of CBTS (Figure 2a), suggests that a 1200 nm thick CBTS absorber used in our PEC devices is able to fully absorb the light with photon energies greater than the CBTS bandgap. The integrated photocurrents from the IPCE data (430−670 nm) are estimated to be 4.0 and 7.2 mA cm^{-2} for bare and CdS/ZnO/TiO_2 modified CBTS photocathodes (Figure S4), respectively, which are similar to those measured from the light linear sweep voltammetry (LSV) scans. The IPCE values are reduced in the wavelength range from 520 to 600 nm, reflecting its absorption nature in this spectral region (Figure 2a). The rapid decay of IPCE curves in the spectral region greater than 600 nm indicates that the absorption onset is approximately 2.05 eV for CBTS, in line with that measured from the optical absorption spectrum and SE. With CdS/ZnO/TiO_2 overlayers, the IPCE values were increased over the entire spectral range. The decrease of IPCE values in the range of 400 to 500 nm is likely due to the absorption from the CdS window layer, which

DOI: 10.1021/acs.chemmater.6b03347
Chem. Mater. XXXX, XXX, XXX−XXX

is known to make no contribution to photocurrents of chalcogenide thin-film solar cells.

The exposed bare CBTS electrode films appear to have only moderate stability under operating conditions (chronoamperometric tests in Figure S5). As seen from the SEM images shown in Figure 4a, the distinct grain morphology of the CBTS film disappeared, and evidence of pitting corrosion on the surface was observed after a long-term (>1 h) PEC testing. However, such pitting did not appear to CBTS electrodes after relatively short-term (~10 min) PEC testing. CBTS films may not be very stable upon exposure to electrolyte solutions for long durations, which is reasonable considering the fact that Cu_2SrSnS_4 can slowly dissolve in water.[36] Another possibility is that the localized change in pH at the electrode surface, resulting from H_2 evolution and production of OH^- ions, may influence the stability of the electrode material. The other possibility is that copious amounts of gas bubbles observed at the film surface act as miniature lenses, causing pitting of the CBTS electrode.[37] As shown in panels (b), (c), and (d) of Figure 4, CdS/ZnO/TiO_2 overlayers can effectively prevent the device from corrosion after long-term PEC tests, because ALD deposited TiO_2 is known to be stable in most electrolyte solutions and has been used to protect various electrode materials.[5,22−24,26−28] The ALD deposition method allows the growth of conformal layers which are both uniform and ultrathin.

In summary, we have shown that the earth-abundant CBTS thin films made via post-sulfurization of co-sputtered sulfide precursors exhibit a bandgap of 2.053 eV with a high absorption coefficient (>10^4 cm^{-1}) and a p-type conductivity. Excitation intensity dependent PL spectral analysis has suggested that the dominant defects in CBTS produce shallow levels and less defect-related band tailing. Moreover, employing CdS/ZnO/TiO_2 overlayers on the CBTS surface can effectively boosts the photocurrent and improves the device stability. The best saturated cathodic photocurrent is enhanced to 7.8 mA cm^{-2} at the potential of −0.10 V versus RHE in a neutral electrolyte solution, as compared to the best bare CBTS thin film attaining a photocurrent of 4.8 mA cm^{-2} at the potential of −0.2 V versus RHE. These results strongly suggest that earth-abundant CBTS is promising as a top-cell absorber for efficient and low-cost tandem polycrystalline thin-film PEC devices, and overlayer engineering can be employed to enhance overall device performances.

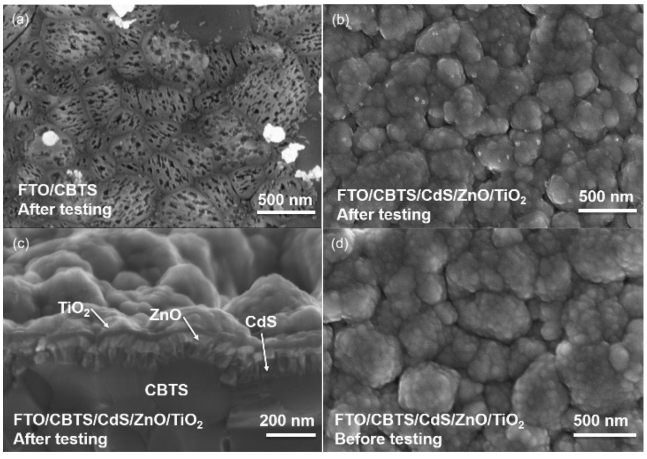

Figure 4. (a) Top-view SEM image of a glass/FTO/CBTS photoelectrode after PEC testing for ~60 min; (b) top-view SEM image of a glass/FTO/CBTS/CdS/ZnO/TiO_2 photoelectrode after PEC testing for ~60 min; (c) magnified cross-sectional SEM image showing the detail at the interface of CBTS/CdS/ZnO/TiO_2 after PEC testing for ~60 min; (d) top-view SEM image of a pristine glass/FTO/CBTS/CdS/ZnO/TiO_2 photoelectrode before PEC testing.

■ ASSOCIATED CONTENT

Supporting Information

The Supporting Information is available free of charge on the ACS Publications website at DOI: 10.1021/acs.chemmater.6b03347.

Experimental details; SE measured dielectric function, refractive index, extinction coefficient, and a best model fit of CBTS; HSE calculated band structure and PDOS for trigonal CBTS; digital photos and chronoamperometric tests of FTO/CBTS and FTO/CBTS/CdS/ZnO/TiO_2 photoelectrodes (PDF)

■ AUTHOR INFORMATION

Corresponding Authors

*E-mail: jie.ge@utoledo.edu (Jie Ge).
*E-mail: yanfa.yan@utoledo.edu (Yanfa Yan).

ORCID

Jie Ge: 0000-0001-5481-4059
Yanfa Yan: 0000-0003-3977-5789

Notes

The authors declare no competing financial interest.

■ ACKNOWLEDGMENTS

The work was supported by the National Science Foundation under Contract No. CHE-1230246 and DMR-1534686. This paper presents results from an NSF project (Award No. CBET-1433401) competitively selected under the solicitation "NSF 14-15: NSF/DOE Partnership on Advanced Frontiers in Renewable Hydrogen Fuel Production via Solar Water Splitting Technologies", which was co-sponsored by the National Science Foundation, Division of Chemical, Bioengineering, Environmental, and Transport Systems (CBET), and the U.S. Department of Energy, Office of Energy Efficiency and Renewable Energy, Fuel Cell Technologies Office. This research also used the resources of the National Energy Research Scientific Computing Center, which is supported by the Office of Science of the U.S. Department of Energy under Contract No. DE-AC02-05CH11231. This work was supported in part by the U.S. Department of Energy, Office of Science, Office of Workforce Development for Teachers and Scientists (WDTS) under the Science Undergraduate Laboratory Internship (SULI) program. Yue Yu and Zewen Xiao are thanked for their support in PEC tests of CBTS photoelectrodes and the calculation of CBTS dielectric functions, respectively.

■ REFERENCES

(1) May, M. M.; Lewerenz, H.-J.; Lackner, D.; Dimroth, F.; Hannappel, T. Efficient Direct Solar-to-Hydrogen Conversion by In Situ Interface Transformation of a Tandem Structure. *Nat. Commun.* **2015**, *6*, 8286.

(2) Brillet, J.; Yum, J.-H.; Cornuz, M.; Hisatomi, T.; Solarska, R.; Augustynski, J.; Graetzel, M.; Sivula, K. Highly Efficient Water Splitting by a Aual-absorber Tandem Cell. *Nat. Photonics* **2012**, *6*, 824−828.

DOI: 10.1021/acs.chemmater.6b03347
Chem. Mater. XXXX, XXX, XXX−XXX

(3) Abdi, F. F.; Han, L.; Smets, A. H. M.; Zeman, M.; Dam, B.; van de Krol, R. Efficient Solar Water Splitting by Enhanced Charge Separation in a Bismuth Vanadate-Silicon Tandem Photoelectrode. *Nat. Commun.* **2013**, *4*, 2195.
(4) Moniz, S. J. A.; Shevlin, S. A.; Martin, D. J.; Guo, Z.-X.; Tang, J. Visible-Light Driven Heterojunction Photocatalysts for Water Splitting - a Critical Review. *Energy Environ. Sci.* **2015**, *8*, 731−759.
(5) Paracchino, A.; Laporte, V.; Sivula, K.; Grätzel, M.; Thimsen, E. Highly Active Oxide Photocathode For Photoelectrochemical Water Reduction. *Nat. Mater.* **2011**, *10*, 456−461.
(6) Li, C.; Hisatomi, T.; Watanabe, O.; Nakabayashi, M.; Shibata, N.; Domen, K.; Delaunay, J.-J. Positive Onset Potential and Stability of Cu_2O-based Photocathodes in Water Splitting by Atomic Layer Deposition of a Ga_2O_3 Buffer Layer. *Energy Environ. Sci.* **2015**, *8*, 1493−1500.
(7) Lee, Y. S.; Chua, D.; Brandt, R. E.; Siah, S. C.; Li, J. V.; Mailoa, J. P.; Lee, S. W.; Gordon, R. G.; Buonassisi, T. Atomic Layer Deposited Gallium Oxide Buffer Layer Enables 1.2 V Open-Circuit Voltage in Cuprous Oxide Solar Cells. *Adv. Mater.* **2014**, *26*, 4704−4710.
(8) Bornoz, P.; Abdi, F. F.; Tilley, D. S.; Dam, B.; van de Krol, R.; Graetzel, M.; Sivula, K. A. Bismuth Vanadate−Cuprous Oxide Tandem Cell for Overall Solar Water Splitting. *J. Phys. Chem. C* **2014**, *118*, 16959−16966.
(9) Dias, P.; Schreier, M.; Tilley, S. D.; Luo, J.; Azevedo, J.; Andrade, L.; Bi, D.; Hagfeldt, A.; Mendes, A.; Grätzel, M.; Mayer, M. T. Transparent Cuprous Oxide Photocathode Enabling a Stacked Tandem Cell for Unbiased Water Splitting. *Adv. Energy Mater.* **2015**, *5*, 1501537.
(10) Hong, F.; Lin, W.; Meng, W.; Yan, Y. Trigonal Cu_2-II-Sn-VI_4 (II = Ba, Sr and VI = S, Se) Quaternary Compounds for Earth-Abundant Photovoltaics. *Phys. Chem. Chem. Phys.* **2016**, *18*, 4828−4834.
(11) Xiao, Z.; Meng, W.; Li, J. V.; Yan, Y. Distant-Atom Mutation for Better Earth-Abundant Light Absorbers: A Case Study of $Cu_2BaSnSe_4$. *ACS Energy Lett.* **2017**, *2*, 29−35.
(12) Bourdais, S.; Choné, C.; Delatouche, B.; Jacob, A.; Larramona, G.; Moisan, C.; Lafond, A.; Donatini, F.; Rey, G.; Siebentritt, S.; Walsh, A.; Dennler, G. Is the Cu/Zn Disorder the Main Culprit for the Voltage Deficit in Kesterite Solar Cells? *Adv. Energy Mater.* **2016**, *6*, 1502276.
(13) Teske, C. L.; Vetter, O. Präparative und Röntgenographische Untersuchung am System $Cu_{2-x}Ag_xBaSnS_4$. *Z. Anorg. Allg. Chem.* **1976**, *426*, 281−287.
(14) Seger, B.; Castelli, I. E.; Vesborg, P. C. K.; Jacobsen, K. W.; Hansen, O.; Chorkendorff, I. 2-Photon Tandem Device for Water Splitting: Comparing Photocathode First versus Photoanode First Designs. *Energy Environ. Sci.* **2014**, *7*, 2397−2413.
(15) Shin, D.; Saparov, B.; Zhu, T.; Huhn, W. P.; Blum, V.; Mitzi, D. B. $BaCu_2Sn(S,Se)_4$: Earth-Abundant Chalcogenides for Thin-Film Photovoltaics. *Chem. Mater.* **2016**, *28*, 4771−4780.
(16) Ge, J.; Grice, C. R.; Yan, Y. Cu-based Quaternary Chalcogenide Cu_2BaSnS_4 Thin Films Acting as Hole-Transport Layers in Inverted Perovskite $CH_3NH_3PbI_3$ Thin-Film Solar Cells. *J. Mater. Chem. A* **2016**, DOI: 10.1039/C6TA08426E.
(17) Ge, J.; Yu, Y.; Yan, Y. Earth-Abundant Trigonal $BaCu_2Sn(Se_xS_{1-x})_4$ (x = 0−0.55) Thin Films with Tunable Band Gaps for Solar Water Splitting. *J. Mater. Chem. A* **2016**, *4*, 18885−18891.
(18) Ge, J.; Koirala, P.; Grice, C. R.; Roland, P. J.; Yu, Y.; Tan, X.; Ellingson, R. J.; Collins, R. W.; Yan, Y. Oxygenated CdS Buffer Layers Enabling High Open-Circuit Voltages in Earth-Abundant Cu_2BaSnS_4 Thin-Film Solar Cells. *Adv. Energy Mater.* **2016**, DOI: 10.1002/aenm.201601803.
(19) Ge, J.; Yu, Y.; Yan, Y. Earth-Abundant Orthorhombic $BaCu_2Sn(Se_xS_{1-x})_4$ ($x \approx 0.83$) Thin Film for Solar Energy Conversion. *ACS Energy Lett.* **2016**, *1*, 583−588.
(20) Vesborg, P. C. K.; Jaramillo, T. F. Addressing the Terawatt Challenge: Scalability in the Supply of Chemical Elements for Renewable Energy. *RSC Adv.* **2012**, *2*, 7933−7947.
(21) Todorov, T.; Gunawan, O.; Guha, S. A Road towards 25% Efficiency and Beyond: Perovskite Tandem Solar Cells. *Mol. Sys. Des. Eng.* **2016**, *1*, 370−376.
(22) Guijarro, N.; Prévot, M. S.; Yu, X.; Jeanbourquin, X. A.; Bornoz, P.; Bourée, W.; Johnson, M.; Le Formal, F.; Sivula, K. A. Bottom-Up Approach toward All-Solution-Processed High-Efficiency $Cu(In,Ga)S_2$ Photocathodes for Solar Water Splitting. *Adv. Energy Mater.* **2016**, *6*, 1501949.
(23) Yang, W.; Oh, Y.; Kim, J.; Jeong, M. J.; Park, J. H.; Moon, J. Molecular Chemistry-Controlled Hybrid Ink-Derived Efficient Cu_2ZnSnS_4 Photocathodes for Photoelectrochemical Water Splitting. *ACS Energy Lett.* **2016**, *1*, 1127−1136.
(24) Luo, J.; Li, Z.; Nishiwaki, S.; Schreier, M.; Mayer, M. T.; Cendula, P.; Lee, Y. H.; Fu, K.; Cao, A.; Nazeeruddin, M. K.; et al. Targeting Ideal Dual-Absorber Tandem Water Splitting Using Perovskite Photovoltaics and $CuIn_xGa_{1-x}Se_2$ Photocathodes. *Adv. Energy Mater.* **2015**, *5*, 1501520.
(25) Naghavi, N.; Abou-Ras, D.; Allsop, N.; Barreau, N.; Bücheler, S.; Ennaoui, A.; Fischer, C. H.; Guillen, C.; Hariskos, D.; Herrero, J.; et al. Buffer Layers and Transparent Conducting Oxides for Chalcopyrite $Cu(In,Ga)(S,Se)_2$ based Thin Film Photovoltaics: Present Status and Current Developments. *Prog. Photovoltaics* **2010**, *18*, 411−433.
(26) Gu, J.; Yan, Y.; Young, J. L.; Steirer, K. X.; Neale, N. R.; Turner, J. A. Water Reduction by a p-$GaInP_2$ Photoelectrode Stabilized by an Amorphous TiO_2 Coating and a Molecular Cobalt Catalyst. *Nat. Mater.* **2016**, *15*, 456−460.
(27) Verlage, E.; Hu, S.; Liu, R.; Jones, R. J. R.; Sun, K.; Xiang, C.; Lewis, N. S.; Atwater, H. A. A Monolithically Integrated, Intrinsically Safe, 10% Efficient, Solar-Driven Water-Splitting System based on Active, Stable Earth-Abundant Electrocatalysts in Conjunction with Tandem III-V Light Absorbers Protected by Amorphous TiO_2 Films. *Energy Environ. Sci.* **2015**, *8*, 3166−3172.
(28) Liang, J.; Tan, H.; Liu, M.; Liu, B.; Wang, N.; Zhang, Q.; Zhao, Y.; Smets, A. H. M.; Zeman, M.; Zhang, X. A Thin-Film Silicon based Photocathode with a Hydrogen Doped TiO_2 Protection Layer for Solar Hydrogen Evolution. *J. Mater. Chem. A* **2016**, *4*, 16841−16848.
(29) Schmidt, T.; Lischka, K.; Zulehner, W. Excitation-Power Dependence of the Near-Band-Edge Photoluminescence of Semiconductors. *Phys. Rev. B: Condens. Matter Mater. Phys.* **1992**, *45*, 8989−8994.
(30) Binsma, J. J. M.; Giling, L. J.; Bloem, J. Luminescence of $CuInS_2$. *J. Lumin.* **1982**, *27*, 55−72.
(31) Unold, T.; Gütay, L. Photoluminescence Analysis of Thin-Film Solar Cells. In *Advanced Characterization Techniques for Thin Film Solar Cells*; Wiley-VCH Verlag GmbH & Co. KGaA: 2011; pp 151−175.
(32) Binsma, J. J. M.; Giling, L. J.; Bloem, J. Luminescence of $CuInS_2$. *J. Lumin.* **1982**, *27*, 35−53.
(33) Levcenko, S.; Tezlevan, V. E.; Arushanov, E.; Schorr, S.; Unold, T. Free-to-Bound Recombination in Near Stoichiometric Cu_2ZnSnS_4 Single Crystals. *Phys. Rev. B: Condens. Matter Mater. Phys.* **2012**, *86*, 045206.
(34) Teixeira, J. P.; Sousa, R. A.; Sousa, M. G.; da Cunha, A. F.; Fernandes, P. A.; Salomé, P. M. P.; Leitão, J. P. Radiative Transitions in Highly Doped and Compensated Chalcopyrites and Kesterites: The Case of Cu_2ZnSnS_4. *Phys. Rev. B: Condens. Matter Mater. Phys.* **2014**, *90*, 235202.
(35) Ge, J.; Chu, J.; Jiang, J.; Yan, Y.; Yang, P. Characteristics of In-Substituted CZTS Thin Film and Bifacial Solar Cell. *ACS Appl. Mater. Interfaces* **2014**, *6*, 21118−21130.
(36) Llanos, J.; Mujica, C.; Buljan, A. Preparation, Transport Properties, and Electronic Structure of Quaternary Sulfides based on Tetrahedral $[MS_4]^{4-}$ Units: $SrCu_2MS_4$ (M = Ge, Sn). *J. Alloys Compd.* **2001**, *316*, 146−152.
(37) Khaselev, O.; Turner, J. A. A Monolithic Photovoltaic-Photoelectrochemical Device for Hydrogen Production via Water Splitting. *Science* **1998**, *280*, 425−427.

DOI: 10.1021/acs.chemmater.6b03347
Chem. Mater. XXXX, XXX, XXX−XXX